# EXPERIMENTAL INVESTIGATION OF SMALL SCALE GEOMETRIES IN A TURBULENT ROUND JET

**M. Gampert, P. Schaefer and N. Peters**
Institute for Combustion Technology
RWTH Aachen University
Templergraben 64, 52056 Aachen, Germany
mgampert@itv.rwth-aachen.de

## ABSTRACT

Based on highly accurate three-dimensional measurements of a scalar field $\theta$, which in the present study is the concentration field of gaseous propane discharging into ambient air from a turbulent round jet, we validate the model equation for the normalized marginal probability density function (pdf) $\tilde{P}(\tilde{l})$ derived by Wang and Peters in the context of dissipation element analysis. Combining a two-dimensional high-speed Rayleigh scattering technique with Taylor's hypothesis allows to resolve the Kolmogorov scale $\eta$ in every spatial direction so that the theoretically derived model equation can be checked against the experimental results at various conditions. We find a very good agreement between theory and experiment and can confirm both, a linear diffusion controlled increase at the origin as well as an exponential tail of the pdf.

## INTRODUCTION

One of the many approaches in turbulence research is to study geometrical structures or characteristic points in the flow field, which allow the extraction of representative information to describe and statistically reconstruct the whole field. [1] analyzed the behaviour at the smallest scales of turbulent scalar fields in terms of the properties of zero gradient points and minimal gradient surfaces. He concluded that these regions of the field are of physical importance to the problem of turbulent mixing.

Based on the extreme points of turbulent scalar fields, i.e. points of vanishing scalar gradient, [2,3] developed the theory of dissipation elements, which arise as natural geometries in turbulent scalar fields, when these are analyzed by means of gradient trajectories. Starting from every grid point, trajectories along the ascending and descending gradient directions can be calculated, which inevitably end in extreme points. All points that share the same two ending points define a finite volume which is called a dissipation element. These elements are parameterized by two values, namely the linear length $l$ between and the scalar difference $\Delta\theta$ at the extreme points. Based on this theory, space filling and non-arbitrary elements are identified, which allow the reconstruction of statistical properties of the field as a whole in terms of conditional statistics within the elements. Examples of such analysis can be found in [3–6]. From the definition of dissipation elements it follows that their temporal evolution in turbulent fields is inherently connected to the evolution of their ending points, which are separated by a mean linear distance $l_m$ of the order of the Taylor microscale $\lambda$ $(= (10k/\varepsilon)^{1/2}$, where $k$ is the turbulent kinetic energy and $\varepsilon$ denotes the energy dissipation rate), see [2]. In addition, direct numerical simulations of homogeneous shear turbulence revealed that a resolution of the order of the Kolmogorov scale $\eta$ is needed to obtain grid independent statistics. As dissipation elements have only been analyzed in simulations so far, an experimental verification is desirable.

Due to their corrugated three-dimensional geometry in combination with the required resolution, an experimental validation is challenging. For a first attempt at comparatively low Reynolds numbers $Re_\lambda$ and resolution using three-simensional measurements of the velocity field in a channel flow obtained via tomographic PIV see [7].

We will study dissipation elements in a passive scalar field $\theta$, which is governed by the convection-diffusion equation

$$\partial\theta/\partial t + u_i(\partial\theta/\partial x_i) = D\partial^2\theta/\partial x_i^2, \tag{1}$$

where $D$ is the constant diffusion coefficient and $u_i$ denotes the velocity component in $i$-direction, while repeated indices imply summation. A wide range of experimental investigations of such a scalar field can be found in the literature, three-dimensional data however is limited as often single- or multi-point measurements in combination with Taylor's hypothesis are conducted, see for instance [8–10], which for obvious reasons are of limited use in the context of dissipation element analysis. The development of advanced laser optical techniques with a high pulse energy at a high repetition rate has facilitated the experimental investigation of spatially three-dimensional conserved scalar quantities. In such measurements, the three-dimensional information is found either by imaging in parallel, spatially distinct two-dimensional planes or via a sweeping of a single two-dimensional laser sheet in sheet normal direction, see [11] for an overview. For the present purpose however, both approaches are impractical

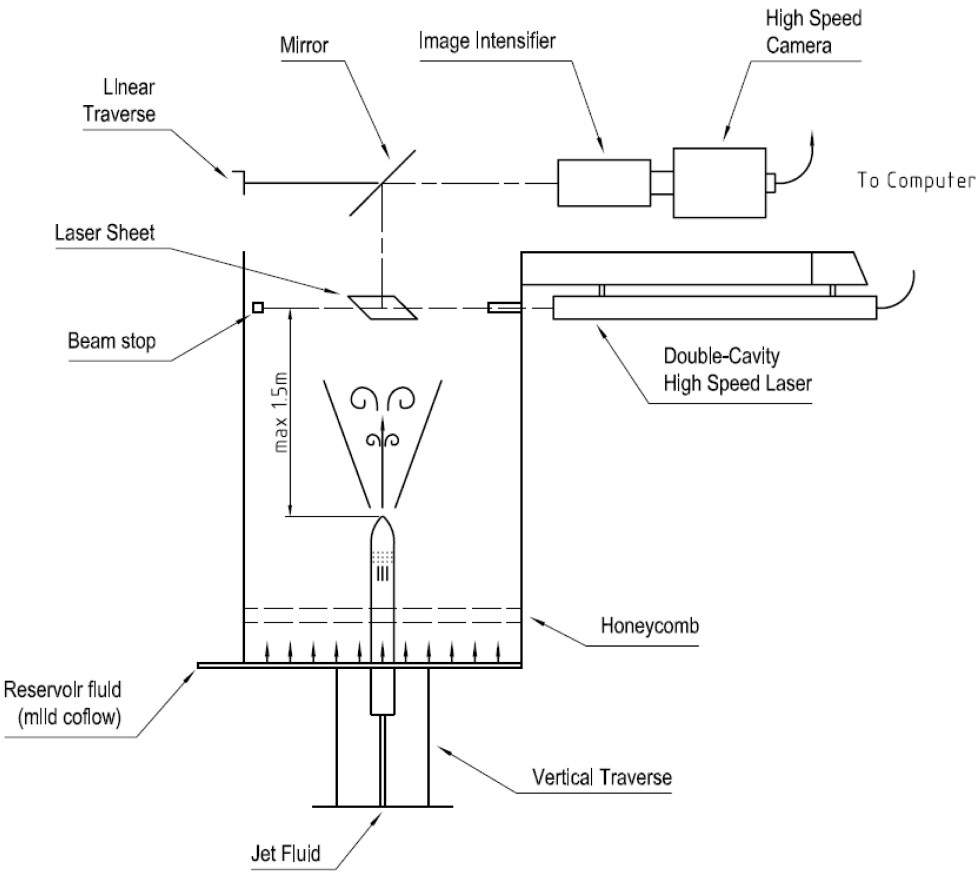


Figure 1. Experimental arrangement of the high-speed Rayleigh system

as in the first one the minimal distance, i.e. the best possible resolution, is limited by the minimal distance between the two planes at which the signals do not interfere. This restriction is not only of importance for dissipation elements, but also creates a severe restriction with respect to accuracy, when three-dimensional gradient quantities in scalar turbulence such as the scalar dissipation rate $\chi$ are considered. The latter is for any dynamically passive, conserved scalar $\theta$ defined as the scalar gradient magnitude squared times the diffusion coefficient $D$, yielding

$$\chi = D(\partial\theta/\partial x_i)^2 = D\left[\left(\frac{\partial\theta}{\partial x}\right)^2 + \left(\frac{\partial\theta}{\partial y}\right)^2 + \left(\frac{\partial\theta}{\partial z}\right)^2\right]. \quad (2)$$

The second approach has been used successfully for measurements in water, see for instance [12], but proves to be difficult in the gas-phase as the Schmidt number $Sc(=\nu/D$, where $\nu$ is the kinematic viscosity), is in liquids roughly three orders of magnitude larger than in the gas-phase. In the next chapter, we will therefore present a method, which combines a high-speed Rayleigh scattering technique with Taylor's hypothesis to resolve the Kolmogorov scale $\eta$ in all three spatial directions, though at moderate Reynolds numbers $Re_\lambda$ ($=u\lambda/\nu$, where $u$ denotes the longitudinal r.m.s. velocity) of $\mathcal{O}(10^2)$. In chapter three, we will give a brief introduction to dissipation elements and validate the marginal pdf $\tilde{P}(\tilde{l})$, before the paper is concluded in chapter four.

## EXPERIMENTAL INVESTIGATION

In the present study, a turbulent round propane jet discharging from a nozzle with a diameter d=6mm into surrounding air has been chosen as the core of the experimental setup. The scalar field, i.e. the concentration of propane, is visualized via Rayleigh scattering of a diode pumped double cavity Nd:YLF laser (Litron Lasers LDY303HE-PIV) at the molecules. The laser emits frequency-doubled light at a wavelength of 527nm, has a pulse energy of 2x22.5mJ with a pulse width of 150ns at 1kHz and can operate at up to 10kHz, see [13] for further information. To account for energy fluctuations, the signal is corrected on a shot by shot basis by a 12bit energy monitor (LaVision Online Energy Monitor).

Laser-Rayleigh scattering is used to determine the instantaneous concentration of the binary mixture of jet and reservoir gas in a small focal plane within the turbulent core of the jet. Laser-Rayleigh scattering has been used and documented in many previous studies, see for instance [10, 14, 15], and is therefore only described briefly here. The technique makes use of the fact that gas molecules elastically scatter photons, and that different molecules have different Rayleigh-scattering cross-sections. In the present study for instance, the cross-section of propane is roughly thirteen times higher than the one of the surrounding air. The signal obtained via

Table 1. Characteristics of the propane jet at various downstream positions

| Case | 1 | 2 | 3 | 4 |
|---|---|---|---|---|
| Downstream position x/d | 30 | 30 | 40 | 40 |
| Jet exit velocity $U_0[m/s]$ | 2.15 | 4.00 | 2.15 | 5.10 |
| $\varepsilon[m^2/s^3]$ | $4.73{\cdot}10^{-2}$ | $3.05{\cdot}10^{-1}$ | $1.78{\cdot}10^{-2}$ | $3.10{\cdot}10^{-1}$ |
| $\bar{\theta}$ | 0.097 | 0.116 | 0.076 | 0.089 |
| Kolmogorov scale $\eta[mm]$ | 0.213 | 0.134 | 0.272 | 0.133 |
| Reynolds number $Re_0$ | 2804 | 5217 | 2804 | 6652 |
| Reynolds number $Re_\lambda$ | 69 | 94 | 69 | 106 |
| Schmidt number $Sc$ | 1.64 | 1.62 | 1.67 | 1.66 |
| Resolution $\Delta x/\eta$ | 0.34 | 0.97 | 0.20 | 0.98 |
| Resolution $\Delta y/\eta = \Delta z/\eta$ | 0.07 | 0.12 | 0.06 | 0.12 |

Rayleigh scattering from a binary gas mixture is related in a linear manner to the concentration $\theta_i$ of the respective gases in the mixture. Considering the gas exiting from the jet to have a concentration in the mixture of $\theta_1$ the two end points $\theta_1$=0 and $\theta_1$=1 of this linear relation are recorded for the calibration, before the conversion from signal to concentration is simply accomplished by linear interpolation.

For the illumination of a two-dimensional plane, a sheet optic for thin, collimated sheets of 130$\mu$m diameter and 25mm height is installed behind laser and energy monitor, thereby illuminating a plane perpendicular to the jet centerline, see fig. 1 for a schematic overview of the full experimental set-up. The resulting signal is recorded with a 12bit LaVision high speed CMOS-camera HighspeedStar6 with a full resolution up to 5.4kHz and 8GB internal memory in combination with a two step high speed intensified relay optic (LaVision HighSpeed IRO). This image intensifier is an electronic shutter device with a maximal repetition rate of 2MHz and an extremely variable exposure time. In contrast to a standard CMOS or CCD, which usually has an exposure time in the *ms* range, the IRO can be operated in the *ns* range, thereby allowing time resolved analysis of shortest light pulses as they are produced by pulsed laser sources. In addition, this IRO has an extremely reduced vignetting, as the light is focused to the image intensifier entrance window, converted to electrons and amplified. Then it is reconverted to light at the exit window, which is focused onto the chip. For further information regarding camera and IRO sensitivity and signal as well as noise considerations see [16, 17].

In order to observe the Rayleigh signal without interaction between optical arrangement and turbulent flow, a mirror is installed in some distance to the laser sheet, which has a thin coating of enhanced aluminium reflecting above 95% of the incomming light at a wavelength of 527nm, thereby minimizing signal losses. To protect the propane jet from exterior influences such as dust particles, a mild co-flow of clean, dry air discharges from a surrounding tube with a diameter of 150mm and a length of 450mm, which guarantees a uniform velocity profile as a honeycomb is installed in the lower third of the tube.

In a next step, the recorded time series of the plane at a fixed downstream position is transformed into a spatial signal based on Taylor's hypothesis, see [18], so that we obtain a frozen three-dimensional concentration field. This approximation estimates the spatial derivative in the streamwise $x$-direction from the local instantaneous value of the time derivative from a single-point or planar measurement, when the required three-dimensional multipoint measurements are impractical or unavailable. In the limit of low turbulence intensities, the motion of gradients relative to the local mean flow can be approximated as one of pure convection. Assuming fluctuations of $\theta$ to be considered frozen over the time scale of the temporal derivative, one obtains

$$\left(\frac{\partial\theta}{\partial x}\right) = -\frac{1}{U}\left(\frac{\partial\theta}{\partial t}\right), \tag{3}$$

or $\Delta x = U\cdot\Delta t$ respectively, where $U$ is the local mean velocity in streamwise direction. Due to the importance of two-point statistics and spatial gradient quantities in turbulence, it is common to use Taylor's hypothesis to estimate spatial derivatives. Even in multipoint probe measurements of velocity gradients, cf. [19, 20], it has been invoked to estimate pdfs and derivatives along the mean streamwise direction.

As the camera can resolve a plane of $1024^2$ pixels at a frequency of 5kHz, this bounds the jet exit velocity $U_0$ to a value, at which the resolution in $x$-direction remains below the Kolmogorov scale. The resulting experimental parameters at two different downstream positions $x/d$ are given in table 1, in which the Taylor based Reynolds number $Re_\lambda$ stems from $Re_\lambda = 1.3\sqrt{Re_0}$ (with $Re_0 = U_0 d/\nu$), cf. [21]. As the jet exit velocity is limited to the respective values, the distance between two recorded images is always below $\eta$ after Taylor's hypothesis is applied. In this relation however, an approximation formula taken from [22] is used to estimate $\varepsilon$. Furthermore, values for the mean scalar value $\bar{\theta}$ and the local

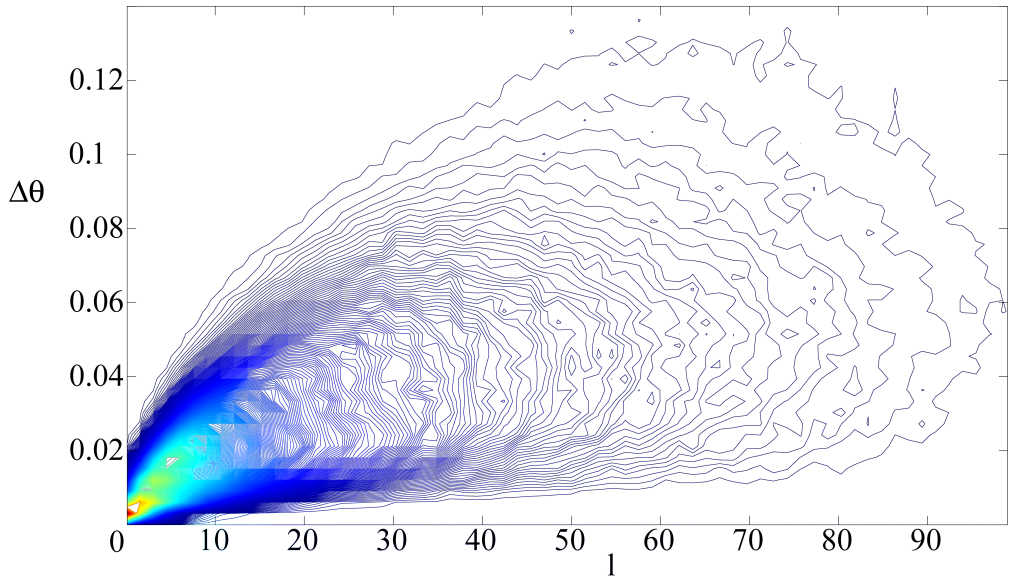


Figure 2. Joint probability density function $P(l,\Delta\theta)$ for case 2 at x/d=30.

Schmidt number $Sc$ are displayed in table 1 to give an impression of the physical parameters.

Based on the raw images recorded by the camera, several corrections of the data are applied before any analysis can be performed. In a first step, noise stemming from dark current and background are subtracted before the intensity of each image is corrected on a shot-by-shot basis to compensate for fluctuations in the laser energy using the energy monitor data as well as for an inhomogeneous illumination in the laser sheet. The size of the images is then reduced from $1024^2$ to $850^2$ to remove areas without signal due to vignetting between IRO and camera. Afterwards, a Mie-filter consisting of an mixed intensity threshold and particle size approach is applied to remove undesirable effects originating from dust particles in the test region. Due to the relatively low jet velocity in combination with the high-speed recording, the signal of a dust particle is captured on several images, once it enters the quadratic area of interest. Based on these corrected images, the signals corresponding to pure air and pure propane respectively are calibrated and used to convert the recorded photon counts to propane concentration. Finally, boxes with a distance $\Delta x = U \cdot \Delta t$ in streamwise direction between two images are formed in which then a three-dimensional diffusion as well as a spectral cut-off filter are applied, before a parallelized trajectory search algorithm is used to identify extreme points and properties of dissipation elements.

## DISSIPATION ELEMENT ANALYSIS

The motivation for dissipation elements is the reconstruction of the entire three-dimensional scalar field by means of an adequate description of an element's characteristics, those being the linear length $l$ and the scalar difference $\Delta\theta$. The corresponding joint probability density function (jpdf) $P(l,\Delta\theta)$ is expected to contain most of the information needed for a statistical reconstruction. Based on a trajectory search algorithm, the passive scalar field has been analyzed for the different experimental cases and the resulting joint pdf for case 2 is shown in figure 2 (to relate the values of $l$ and $\Delta\theta$ given in this figure to other characteristic flow quantities see table 1). In this illustration, different physical effects are illustrated. Besides a distinct maximum, one observes a decrease at the origin, corresponding to the annihilation of small elements due to molecular diffusion. The region in the upper right hand area of the jpdf is dominated by extensive strain, as large elements are exposed to large velocity differences.

This jpdf can be described by a model equation. Based on Bayes theorem, it is decomposed into a marginal pdf $P(l)$ of the linear distance and a conditional pdf $P(\Delta\theta \mid l)$ of the scalar difference, yielding

$$P(l,\Delta\theta) = P(l)\, P(\Delta\theta \mid l), \tag{4}$$

where the marginal pdf $P(l)$ is defined by

$$P(l) = \int_0^\infty P(\Delta\theta, l)\, d\Delta\theta. \tag{5}$$

For this pdf in its normalized form $\tilde{P}(\tilde{l})$, with $\tilde{P} = P\, l_m$ and $\tilde{l} = l/l_m$, the following model equation was derived in [3]

$$\frac{\partial \tilde{P}(\tilde{l},\tilde{t})}{\partial \tilde{t}} + \frac{\partial}{\partial \tilde{l}}(\tilde{P}(\tilde{l},\tilde{t})[\tilde{v}_D(\tilde{l}) + \tilde{a}(\tilde{l})\tilde{l}]) = \Lambda_s \int_{\tilde{l}}^\infty \tilde{P}(\tilde{z},\tilde{t})\, d\tilde{z} - \Lambda_a \tilde{l}\tilde{P}(\tilde{l},\tilde{t}). \tag{6}$$

In this equation, $\tilde{a}$ represents the conditional mean strain rate $a$ of the elements of length $l$

$$a = \frac{< \Delta u_n \mid l >}{l}, \tag{7}$$

where $\Delta u_n$ denotes the velocity difference at the ending points projected in direction of the linear connecting line, normalized by its asymptotic value $a_\infty$, which is approached for $l \to \infty$. Furthermore, $\tilde{v}_D$ is defined as

$$\tilde{v}_D = v_D/(l_m\, a_\infty) = -4D/l\left(c\,\tilde{l}\,exp(-\tilde{l})\right)/(l_m\, a_\infty), \tag{8}$$

and denotes the normalized drift velocity due to molecular diffusion in eq. 6. It is responsible for the linear decrease of $\tilde{P}(\tilde{l})$ for $\tilde{l} \to 0$ as will be shown below. The constant $c$ in eq. 8 is determined from the condition that the total length of the array must not change, cf. [3], and $D$ is the molecular diffusion coefficient. In addition in eq. 6 the two non-dimensionalized numbers $\Lambda_s$ and $\Lambda_a$ appear. These describe the splitting (respectively reconnection) of larger (smaller) elements into smaller (larger) ones and are determined from the normalization and the first moment during the solution of the equation as eigenvalues of the problem, cf. [23]. Eq. 6 can be solved numerically and will be compared to the experimental results in the following as it is considered to be independent of the Reynolds number and type of turbulent flow, cf. [6] for a detailed discussion.

Figures 3-6 depict the results for the normalized pdf of the length distribution $\tilde{P}(\tilde{l})$ obtained at the different downstream positions and jet exit velocities given in table 1. In general, one observes a very good agreement of the experimental results with the solution of the theoretically derived model. Slight differences can be identified at x/d=40, where the maximum of the experimentally obtained length distribution is slightly tilted to the left and small deviations in the exponential tail can be identified. The maximal value of the pdf however, is well described by the model solution and the linear increase at the origin as well as the exponential tail, see especially the log-insets, follow closely the predicted solution. In addition, figures 3-6 illustrate that the equation for $\tilde{P}(\tilde{l})$ seems not to be a function of the Reynolds number as the values of $R_\lambda$ vary roughly between 70 and 100, so that

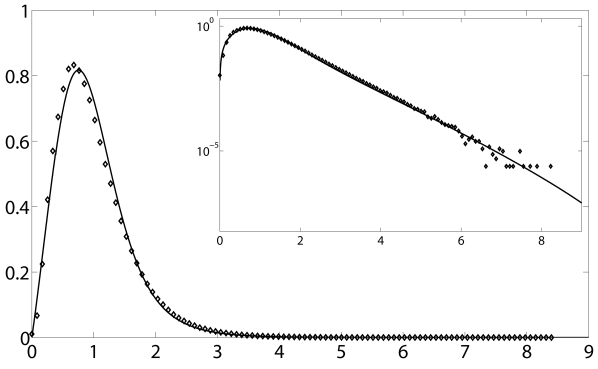

Figure 3. Marginal pdf $\tilde{P}(\tilde{l})$ for case 1

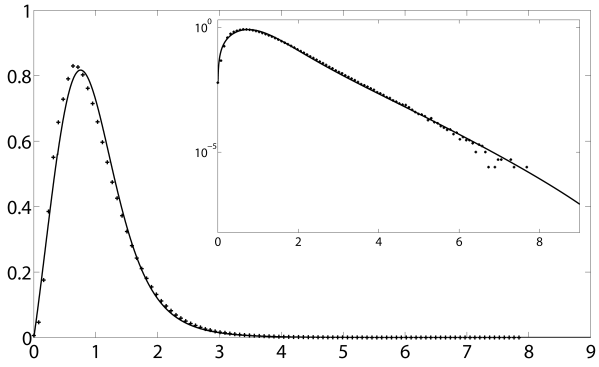

Figure 4. Marginal pdf $\tilde{P}(\tilde{l})$ for case 2

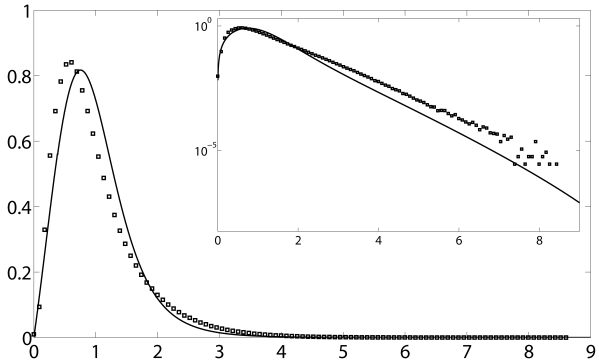

Figure 5. Marginal pdf $\tilde{P}(\tilde{l})$ for case 3

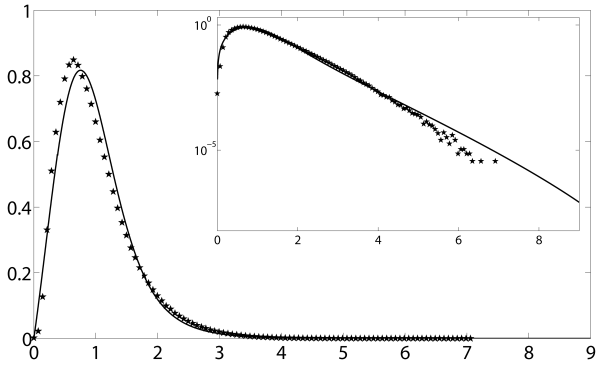

Figure 6. Marginal pdf $\tilde{P}(\tilde{l})$ for case 4

the shape of the non-dimensional marginal pdf $\tilde{P}(\tilde{l})$ and its model equation may be considered independent from inhomogeneities and anisotropies, a finding which is in good agreement with the results obtained in [6].

## CONCLUSION

Based on three-dimensional measurements of the concentration field at different downstream positions around the center line of a turbulent round jet, we have presented detailed experimental validation for the theoretically derived marginal pdf for the length of dissipation element. Overall, we find an excellent agreement between model and experimental data. In

particular, the linear increase at the origin due to diffusion as well as the exponential tail stemming from the Poisson process employed in the derivation can be confirmed by the present data. Finally, no dependance on the Reynolds number is implied by the results, which is in good agreement with theory and numerical results.

## ACKNOWLEDGEMENTS

This work was funded by the NRW-Research School "BrenaRo" and the Cluster of Excellence "Tailor-Made Fuels from Biomass", which is funded by the Excellence Initiative of the German federal state governments to promote science and research at German universities.

## REFERENCES

[1] C. H. Gibson, "Fine structure of scalar fields mixed by turbulence i. zero gradient points and minimal gradient surfaces," *Phys. Fluids*, vol. 11, pp. 2305–2315, 1968.

[2] L. Wang and N. Peters, "The length scale distribution function of the distance between extremal points in passive scalar turbulence," *J. Fluid Mech.*, vol. 554, pp. 457–475, 2006.

[3] L. Wang and N. Peters, "Length scale distribution functions and conditional means for various fields in turbulence," *J. Fluid Mech.*, vol. 608, pp. 113–138, 2008.

[4] P. Schaefer, M. Gampert, J. H. Goebbert, L. Wang, and N. Peters, "Testing of different model equations for the mean dissipation using Kolmogorov flows," *Flow, Turbulence and Combustion*, vol. 85, pp. 225–243, 2010.

[5] P. Schaefer, M. Gampert, M. Gauding, N. Peters, and C. Treviño, "The secondary splitting of zero gradient points in a turbulent scalar field," *J. Eng. Math.*, pp. DOI: 10.1007/s10665–011–9452–x, 2011.

[6] M. Gampert, J. Goebbert, P. Schaefer, M. Gauding, N. Peters, F. Aldudak, and M. Oberlack, "Compressive and extensive strain along gradient trajectories in the turbulent kinetic energy field," *accepted for publication in New J. of Physics*, 2011.

[7] L. Schaefer, U. Dierksheide, M. Klaas, and W. Schroeder, "Investigation of dissipation elements in a fully developed turbulent channel flow by tomographic particle-image velocimetry," *Phys. Fluids*, vol. 23, p. 035106, 2010.

[8] R. A. Antonia, E. Hopfinger, Y. Gagne, and F. Anselmet, "Temperature structure functions in turbulent shear flows," *Physical Review A*, vol. 30, pp. 2704–2707, 1984.

[9] L. Mydlarski and Z. Warhaft, "Passive scalar statistics in high-péclet-number grid turbulence," *J. Fluid Mech.*, vol. 358, pp. 135–175, 1998.

[10] B. Talbot, N. Mazellier, B. Renou, L. Danaila, and M. Boukhalfa, "Time-resolved velocity and concentration measurements in variable-viscosity turbulent jet flow," *Exp. Fluids*, vol. 47, pp. 769–787, 2009.

[11] L. K. Su and N. T. Clemens, "Planar measurements of the full three-dimensional scalar dissipation rate in gas-phase turbulent flows," *Exp. Fluids*, vol. 27, pp. 507–521, 1999.

[12] R. Miller, L. Dasi, and D. Webster, "Multipoint correlations of concentration fluctuations in a turbulent passive scalar," *Exp Fluids*, vol. 44, pp. 719–732, 2008.

[13] LitronLasers, "Ldy300piv," *Litron Lasers Ltd; Warwickshire, England*, 2010.

[14] D. R. Dowling and P. E. Dimotakis, "Similarity of the concentration field of gas-phase turbulent jets," *J. Fluid. Mech.*, vol. 218, pp. 109–141, 1990.

[15] L. K. Su and N. T. Clemens, "The structure of fine-scale scalar mixing in gas-phase planar turbulent jets," *J. Fluid Mech.*, vol. 488, pp. 1–29, 2003.

[16] LaVision, "Product manual highspeed iro," *LaVision GmbH, Göttingen*, 2007.

[17] LaVision, "Product manual highspeedstar6," *LaVision GmbH, Göttingen*, 2008.

[18] G. I. Taylor, "The spectrum of turbulence," *Proc. R. Soc.London Ser. A*, vol. 164, p. 476, 1983.

[19] A. Tsinober, E. Kit, and T. Dracaos, "Experimental investigation of the field of velocity gradients in turbulent flows," *J. Fluid Mech.*, vol. 242, p. 169, 1992.

[20] M. Kholmyansky and A. Tsinober, "On an alternative explanation of anomalous scaling and how well-defined is the concept of inertial range," *Phys. Letters A*, vol. 373, pp. 2364–2367, 2009.

[21] J. Peinke, C. Renner, and F. R, "Experimental indications for markov properties of small-scale turbulence," *J. Fluid Mech.*, vol. 433, pp. 383–409, 2001.

[22] C. A. Friehe, C. W. V. Atta, and C. H. Gibson, "Jet turbulence dissipation rate measurements and correlations," *AGARD Turbulent Shear Flows*, vol. CP-93, pp. 18.1–18.7, 1971.

[23] P. Schaefer, M. Gampert, L. Wang, and N. Peters, "Fast and slow changes of the length of gradient trajectories in homogenous shear turbulence," in *Advances in Turbulence XII* (B. Eckhardt, ed.), pp. 565–572, Springer-Verlag, Berlin Heidelberg New York Tokyo, 2009.